CICE 2025
12th International Conference on FRP Composites in Civil Engineering
14–16 July, 2025, Lisbon

INFLUENCE OF SURFACE CONDITIONS AND EMBEDMENT LENGTH ON THE BOND-SLIP RESPONSE OF GFRP REBARS IN CONCRETE

João Pacheco de Almeida[1a], Ryan Hoult[1b] and Alexander Zoller[2c]

[1]Institute of Mechanics, Materials and Civil Engineering, UCLouvain, Belgium
E-mail: [a]joao.almeida@uclouvain.be, [b]ryan.hoult@uclouvain.be
[2]Arkema, France
E-mail: [c] alexander.zoller@arkema.com

Abstract
Reinforcing concrete members with fibre-reinforced polymer (FRP) rebars, as an alternative to common corrosion-prone steel rebars, is steadily increasing, leveraging on their potential to ensure longer structural service lives. Another boost will come from the second generation of Eurocode 2, which for the first time includes supplementary guidance for the design of new structures with non-prestressed glass and carbon fibre reinforcement. Several technological developments are ongoing to optimize the performance of FRP rebars, namely regarding their surface and bond-slip response. This topic is investigated herein via an experimental program focusing on two complementary aspects: (i) the influence of various surface conditions on the bond stress-slip behaviour of glass FRP (GFRP) rebars with thermoset and thermoplastic polymers; machine-coated and helically-wrapped sand-coated surfaces are included, as well as newer approaches to surface treatment such as peel-ply and peel-ply/grid; (ii) the influence of different embedment lengths, namely 10×, 20×, and 30× the rebar diameter, on the pull-out response of GFRP rebars with a yet-distinct surface treatment known as calendering; this paper briefly shows and discusses the evolution of strains along the three embedment lengths up until pull-out failure, as obtained from distributed optical fibre sensors, which is another novelty.

Keywords: GFRP reinforcement; Rebar surface; Bond-slip; Reinforced concrete; Distributed optical fibre sensors.

1. Introduction

In recent years, technological improvements have led to the development of innovative Glass Fiber Reinforced Polymer (GFRP) rebar surfaces, featuring specialised coatings and textures designed to improve the bond with surrounding concrete. This study presents an experimental campaign with two interrelated objectives. The first is to evaluate the bond-slip behavior of GFRP reinforcement ("rebars") with various surface treatments, including new approaches to surface finishing, namely for thermoplastic rebars. The second is to examine the effect of different embedment lengths on the slip mechanism and failure modes. The experiments were conducted at the LEMSC laboratory (Laboratory for Mechanical Testing, Structures, and Civil Engineering) within the IMMC (Institute of Mechanics, Materials, and Civil Engineering) at Université catholique de Louvain (UCLouvain), Belgium. The present manuscript corresponds to a highly abridged version of a manuscript currently under review [1].

Various surface treatment methods can be employed to enhance the adhesion to concrete. These treatments can generally be applied to both thermoset and the more recent thermoplastic rebars. The latter can be reshaped and recycled by reheating. The following is a summary of the available options: (i) helically wrapped rebars: these rebars feature a helical wrap around their surface, creating a mechanical interlock with the concrete that significantly enhances bond strength. The wrap, typically composed of fibers or resins, is applied during the manufacturing process; (ii) sand-coated rebars: a layer of sand particles is bonded to the rebar surface while the resin is still tacky. This coating substantially increases friction between the rebar and concrete; (iii) ribbed rebars: similar to traditional steel rebars, these have grooves or ribs on their surface that provide a robust mechanical interlock; (iv) machine-coated rebars: specialized coatings are applied using automated machinery. The process ensures uniform application for consistent performance; (v) for thermoplastic GFRP rebars, an additional method is calendering, where the bar passes through a roller with a textured surface immediately after the pultrusion die. This process creates a slightly deformed and roughened surface, promoting better adhesion to concrete; (vi) other newer techniques, such as peel-ply and peel-ply/grid, involve applying a surface layer that can later be peeled off to leave a roughened texture or grid-like structure for improved bond. These latter methods, along with calendering, are scarcely explored in the existing literature but are examined in the present study. For instance, they cannot be found in the recent large database assembled by Wang *et al.* [2], which will be employed in this study. While some initial studies [3] pointed to a negligible effect on the bond strength of FRP bars to concrete, more recent studies [4], [5] unsurprisingly demonstrate the **complex effect of the bar surface on characteristics of bond behaviour**, as well as considerable bond strength variation within the same surface type. Sand-coated (SC) bars rely on chemical adhesion and friction, with bond strength depending on the sand's properties. Helically wrapped (HW), ribbed (RB), and indented (IN) bars primarily use mechanical interlocking with concrete. Combining treatments, helically wrapped with sand coating (HWSC) and indented with sand coating (INSC) bars exhibit intermediate behaviours. The effectiveness of each treatment also depends on factors like the concrete strength, concrete cover, bar diameter d_b, and embedment length [6].

Regarding the latter, the literature shows that **a larger embedment length generally leads to a decrease in the average bond strength** [7] due to the non-linear distribution of bond stress [8] and the Poisson effect [6]. Zhao et al. [2] hence postulated that resin micro-damage and friction gave contributions to the peak load that depended on the bonded length. They also found that design codes like ACI 440.1R-15 may be excessively conservative in specifying development lengths, since their experiments showed that a $40d_b$ length was sufficient to reach failure, while ACI requires around $80d_b$.

2. Summary of Experimental Program

2.1. Rebar surface conditions and specimen identification

Six types of GFRP rebars are considered in the present study. They differ in surface condition, diameter, and resin composition. Following the order of presentation in Figure 1: (i) calendered rebars (acronym: Cal) with a 13-mm nominal diameter and the smoothest surface finish herein considered; (ii) machined 13-mm bars (acronym: Mach), with a distinctive ribbed surface profile; (iii) peel-ply bars (acronym: PL) with a diameter of 16 mm; (iv) peel-ply/grid 13-mm rebars (acronym: PLG); lastly, sand-coated rebars rebars (acronym: SC) with a wrapped helical strand and two different diameters: (v) 13 mm (SC13), and (vi) 16 mm (SC16). Concerning the resin type, the sand-coated rebars use a thermosetting polymer, Vinyl Ester, while all the remaining rebar types employ Elium® C599 E [9], a thermoplastic resin.

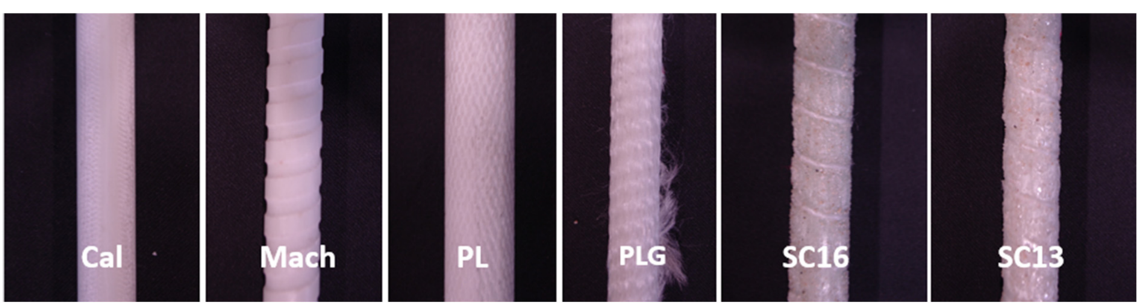

Figure 1. Tested GFRP rebar surface types: CALendered (Cal), MACHined (Mach), PL (PeeL-ply), PeeL-ply/Grid (PLG), and helically-wrapped Sand-Coated (SC) with diameters of 16 and 13 mm.

Table 1. Identification of GFRP rebar specimens (surface type-embedment length-sample)

Calendered	Peel-ply/grid	Machined	Sand-coated	Peel-ply
Cal-10d_b-1	PLG-4d_b-1	Mach-4d_b-1	SC13-4d_b-1	PL-4d_b-1
Cal-10d_b-2	PLG-4d_b-2	Mach -4d_b-2	SC13-4d_b-2	PL-4d_b-2
Cal-10d_b-3	PLG-4d_b-3	Mach -4d_b-3	SC13-4d_b-3	PL-4d_b-3
Cal-10d_b-4	PLG-4d_b-4	Mach -4d_b-4	SC13-4d_b-4	PL-4d_b-4
Cal-20d_b-1			SC16-4d_b-1	
Cal-20d_b-2			SC16-4d_b-2	
Cal-20d_b-3			SC16-4d_b-3	
Cal-30d_b-1			SC16-4d_b-4	
Cal-30d_b-2				
Cal-30d_b-3				

The specimens tested in this experimental program, summarized in Table 1, are labeled using the notation X-Y-Z. Here, X refers to the rebar type as mentioned above, Y denotes the embedment length expressed as a multiple of the rebar diameter d_b (specifically 4d_b, 10d_b, 20d_b, and 30d_b), and Z identifies the specific sample within each X-Y group. The cubic samples and experimental setup for the specimens with a length of 4d_b, which are used to test the influence of the surface conditions, are described in the following section. The cylindric samples and setup for the specimens with embedment lengths of 10d_b, 20d_b, and 30d_b, employed to investigate the effect of the embedment length, are explained in Section 2.3. A 1000 kN MTS tension test machine was used for all tests.

2.2. Influence of surface conditions: setup and instrumentation

Referring to Figure 2(a), the cubic samples discussed in this study correspond to an embedment length of $L_e = 4d_b$. For the GFRP rebars used, which have a maximum diameter of 16 mm, the standard ISO 10406-1 (2015) specifies the use of concrete cubes with side lengths H = 100 mm. Consequently, the unbonded length of the rebar (L_{PVC}), achieved using a PVC sleeve, varied as follows: L_{PVC} = 48 mm for d_b = 13 mm and L_{PVC} = 36 mm for d_b = 16 mm. The length a, which must exceed both 300 mm and 40d_b, was governed by the latter condition, resulting in a = 520 mm for d_b = 13 mm and a = 640 mm for d_b = 16 mm. The code-prescribed free length e of 10 mm was also maintained.

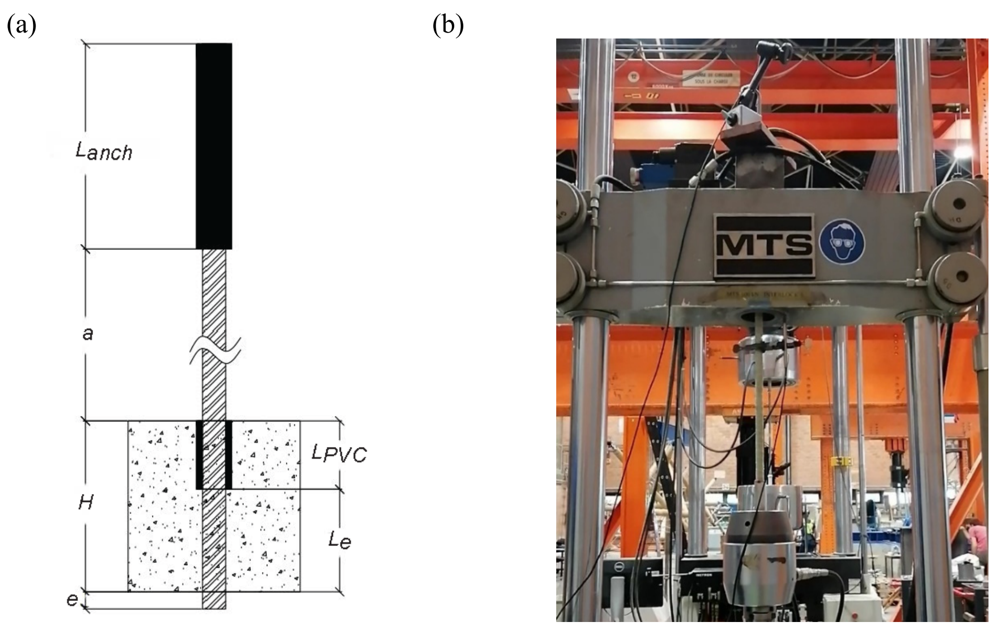

Figure 2. (a) Geometric details of cubic samples with embedment length of 4d_b; (b) Test setup.

To prevent splitting failure of the concrete, each sample included a steel 6-mm spiral reinforcement with an external diameter of 80 mm and a pitch of 40 mm. The casting was performed horizontally, and the samples were subsequently submerged in a water tank under controlled temperature conditions until the day of testing, following the recommendations of ISO 10406-1 (2015). Compressive tests conducted on three 150×300 mm cylinders at 28 days yielded an average strength of 38 MPa, which slightly exceeded the standard range of 30±3 MPa. The experimental setup for the cubic samples also followed the guidelines outlined in the ISO standard [10], as depicted in Figure 2(b). A linear variable differential transformer (LVDT) measured the displacement of the free-end of the rebar. Finally, again in accordance with the abovementioned standard, an average loading speed of 2.5 kN/min was applied.

2.3. Influence of embedment length: setup and instrumentation

To examine the effect of embedment length on bond stress, cylindrical samples with calendered rebars of 13 mm diameter were tested. Embedment lengths of $L_e = 10d_b$ (130 mm), $L_e = 20d_b$ (260 mm), and $L_e = 30d_b$ (390 mm) were investigated. The cylinders had a diameter of 200 mm, with a height comprising the embedment length and a fixed unbonded length of $L_{PVC} = 100$ mm, achieved using a PVC sleeve, as illustrated in Figure 3(a). The free-end length extending beyond the cylinder was set to $e = 50$ mm, while length a was 600 mm, 470 mm, and 340 mm for cylinders with $L_e = 10d_b$, $20d_b$, and $30d_b$, respectively.

Two concrete batches were prepared. The first was used for samples with $L_e = 10d_b$ and for samples Cal-$20d_b$-2 and Cal-$20d_b$-3. The second batch was used for $L_e = 30d_b$ and sample Cal-$20d_b$-1. Compressive tests on three cylinders from the first batch (at 25 days) yielded an average strength of 32 MPa, within the target range. Conversely, tests on two cylinders from the second batch (at 24 days) showed a higher average strength of 41 MPa, exceeding the standard range of 30±3 MPa. The cylindrical samples were subjected to displacement-controlled loading at a constant rate of 0.02 mm/s. Two LVDTs were used to measure displacement at the loaded and free ends of the specimens. An extensometer, affixed to the rebar over a 100 mm gauge length, captured local elongation. Finally, three specimens (Cal-$10d_b$-3, Cal-$20d_b$-1, and Cal-$30d_b$-1) were outfitted with distributed fibre optic sensors (DFOS) to monitor strain distribution along the GFRP rebars [11]. The sensors were adhered to the rebar and operated with a LUNA interrogator (ODiSI 6104 Series) at a spatial resolution of 0.65 mm and a frequency of 12.5 Hz. The strain data was processed using a moving average filter over the central 10 data points (roughly 6.5 cm); any missing data (NaN) was linearly interpolated between the surrounding non-NaN values.

(a) (b)

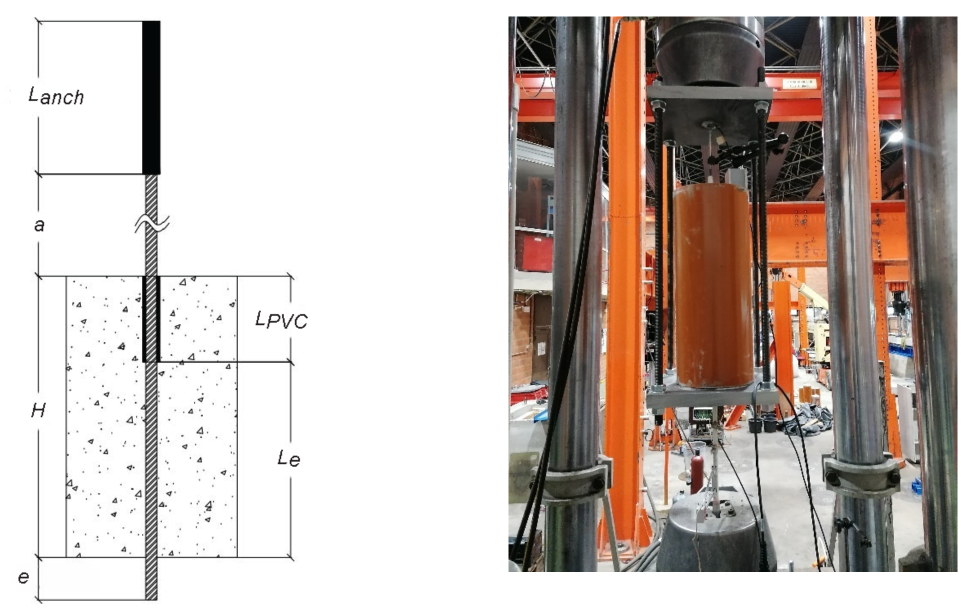

Figure 3. (a) Geometric details of cylindric samples with embedment lengths of $10d_b$, $20d_b$, and $30d_b$; (b) Test setup.

3. Influence of Surface Conditions

3.1. Experimental results

The test results obtained with the cubic samples are shown in Figure 4, grouped according to the rebar diameter (i.e., 13 mm or 16 mm). All specimens failed through pull-out, characterized by the slippage of the bar relative to the concrete cylinder. Following the tests, the specimens were split for visual inspection, revealing that several exhibited a highly moist concrete interface around the reinforcing bar, which appeared to diminish the rebar-concrete bond artificially. Therefore, Figure 4 includes only pull-out results for the specimens with clear traces of observed concrete moisture around the pulled-out rebar. Two pairs of graphs are included (one for each diameter, with distinct vertical axes' upper limits), depicting: (i) the loaded-end force, as measured by the MTS tension testing machine, plotted against the corresponding stroke; and (ii) the average bond stress plotted against the free-end slip. The average bond stress is determined by dividing the tensile force at the loaded end by the bonded surface area between the rebar and the surrounding concrete. The stroke displacements recorded by the testing machine were notably larger than those captured by the free-end LVDT, which had a limited displacement range (shown until 7 mm in Figure 4). To facilitate the connection between the graphs, identical-colour markers were plotted for each pair of graphs, for every rebar surface type, indicating the same loading instant. The main measured quantities are shown in Table 2, which includes the maximum force, the bond strength $\boldsymbol{\tau_{max}}$ (obtained as the maximum of the average bond stress), and the value of slip corresponding to the bond strength, $\boldsymbol{s_{max}}$.

Due to space limitations, only some brief relevant conclusions are included herein from the test of cubic samples with an embedment length of $4d_b$: (i) there is a substantial impact of the surface treatment on $\boldsymbol{\tau_{max}}$ – a four-fold increase from 2.96 MPa (PLG-$4d_b$-3) to 12.23 MPa (SC16-$4d_b$-1), as well as on $\boldsymbol{s_{max}}$; (ii) helically-wrapped sand-coated rebars with 16-mm diameter exhibited the highest bond strength; however, the comparison between SC16 and SC13 reveals that this significant rebar-diameter-effect is opposite to findings from previous studies [12] and hence warrants further investigation; (iii) the variability of the bond strength $\boldsymbol{\tau_{max}}$ within the different samples, i.e. for the same surface, is also noteworthy, particularly for the rebars with peel-ply/grid and the 13-mm helically wrapped sand-coating. A much-extended and thorough analysis can be consulted in another reference [1].

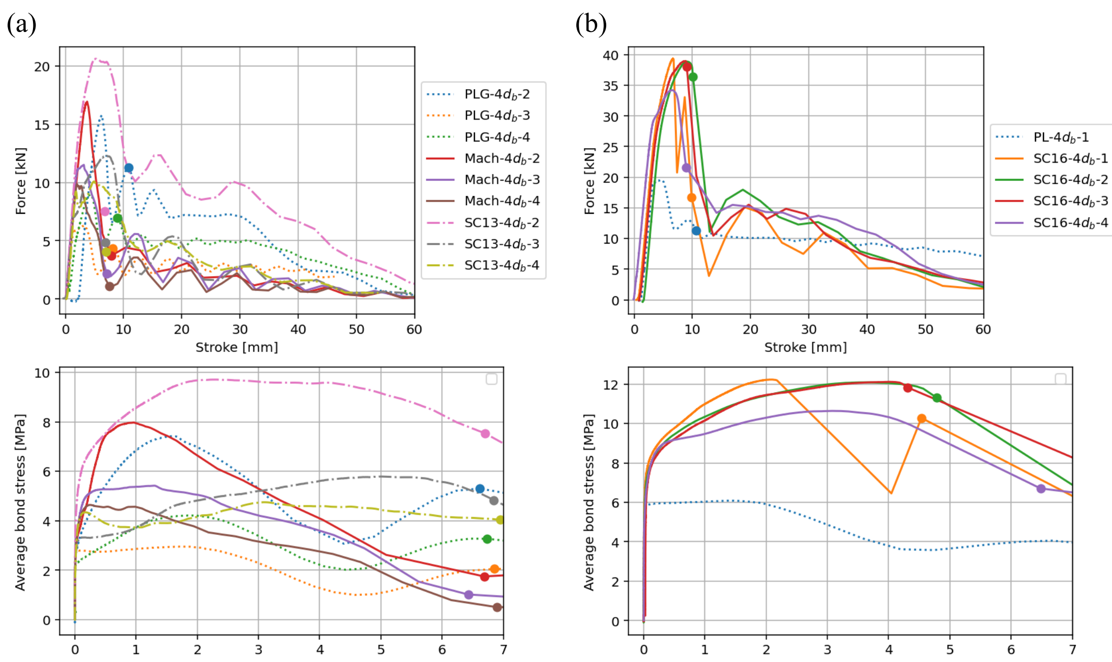

Figure 4. Validated cubic-sample pull-out results for rebars with diameter: (a) 13 mm; (b) 16 mm.

Table 2. Summary of validated pull-out results for cubic samples

Unit	d_b [mm]	F_{max} [kN]	τ_{max} [MPa]	s_{max} [mm]
PLG-4d_b-2	13	15.76	7.42	1.59
PLG-4d_b-3		6.28	2.96	1.77
PLG-4d_b-4		8.95	4.21	1.85
PL-4d_b-1	16	19.57	6.08	1.37
Mach-4d_b-2	13	16.93	7.97	0.96
Mach-4d_b-3		11.51	5.42	1.30
Mach-4d_b-4		9.86	4.64	0.24
SC16-4d_b-1	16	39.35	12.23	2.08
SC16-4d_b-2		38.88	12.09	3.59
SC16-4d_b-3		38.97	12.11	4.02
SC16-4d_b-4		34.22	10.64	3.08
SC13-4d_b-2	13	20.62	9.71	2.30
SC13-4d_b-3		12.29	5.79	5.02
SC13-4d_b-4		10.09	4.75	3.11

3.2. Comparison with literature

This section compares the bond strength results herein obtained with those from a recent database compiled by Wang et al. [6]. The latter includes 407 pull-out test results from the literature, encompassing different types of fibers, concrete strengths, bar diameters, embedment lengths, and concrete covers. The surface properties of the FRP bars in the database were classified into sand-coated (SC), helically wrapped, ribbed, indented, helically wrapped with sand coating (HWSC), and indented with sand coating. Hence, some surface treatment types tested in the present investigation (namely calendering, peel-ply, and peel-ply/grid) cannot be found in this database. Figure 5(a) situates the bond strength obtained for the present 14 cubic samples within said database. The data points in grey include other results obtained in the present experimental campaign, but not discussed herein [1]. The plot is expressed in terms of the concrete strength square root, which is found to have a positive correlation for most concrete grades. Slight horizontal random offsets are applied to all markers along vertical lines with concentration of datapoints (since the database has many test results with identical concrete strength), for a clearer visualization. It is observed that the current bond strength results are, overall, on the lower side, which could point to an overall bias of the test campaign. The peel-ply and peel-ply/grid specimens are even among the lowest data points in the entire database. Figure 5(b) plots the results against the rebar diameter, highlighting in green and yellow the database entries corresponding to SC and HWSC rebars. Again, the data points are displayed with slight horizontal offset to reduce overlap corresponding to results with identical diameter. The linear regression for the entries SC13 and SC16 in the current study (which correspond, in fact, to helically-wrapped sand-coated bars, HWSC) exhibits an opposite trend compared to the regression lines drawn for the rest of the database, as discussed before.

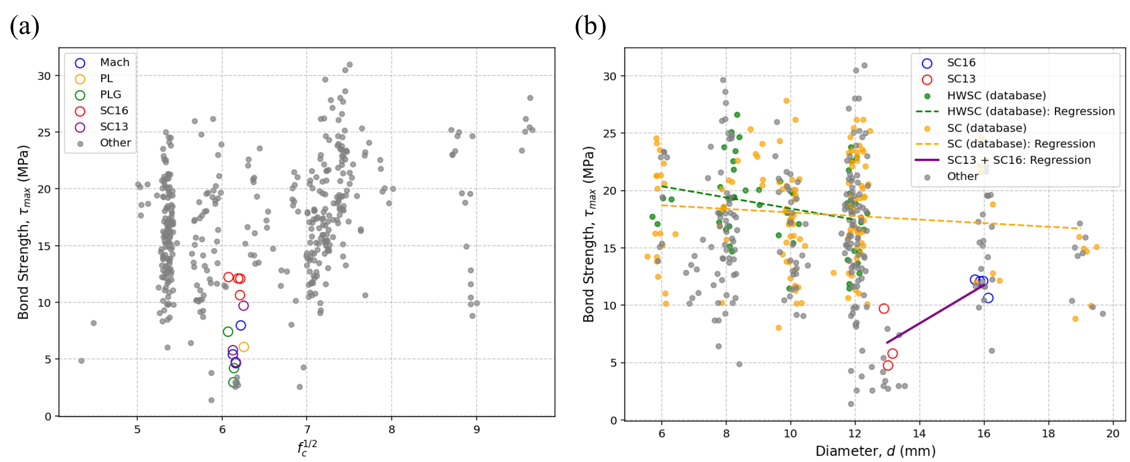

Figure 5. Comparison of bond strength results as obtained from the current cubic-sample test program and from the literature, plotted against: (a) the concrete strength square root; (b) the diameter.

4. Influence of Embedment Length

Figure 6(a) and (b) show the force *versus* stroke and the average bond stress *versus* free-end slip, for the three calendered rebars instrumented with DFOS and embedment lengths of 10d_b (130 mm), 20d_b (260 mm), and 30d_b (390 mm). Similarly to the cubic units, these specimens failed through pull-out. The peak force for units Cal-10d_b-3, Cal-20d_b-1, and Cal-30d_b-1, was 25.05 kN, 46.91 kN, and 54.75 kN, respectively; the resulting bond strength for the same three specimens was 4.89 MPa, 4.42 MPa, and 3.44 MPa, respectively. These results are representative of a clear trend for all the ten calendered rebars tested (not shown here, please refer to [1]): the bond strength reduces as the embedment length increases.

Figure 6(c) shows, with solid lines, the strain distribution along the GFRP rebars at the abovementioned pull-out peak force for each specimen. For the specimen with the smallest embedment length (10d_b), the strain distribution at pull-out capacity is approximately linear. As the embedment length increases, i.e. for 20d_b and 30d_b, the strain profiles at pull-out capacity present an increasingly nonlinear shape, becoming flatter near the rebar loaded end; this signals a reduction of the bond stress in this region. Figure 6(c) also shows that, at identical values of maximum strain at the loaded end (i.e., for approximately similar values of pull-out force), for larger embedment lengths, the strain profiles are spread out over longer segments of the rebar. Interestingly, this appears to occur even when the unloaded end of the rebars are still unstrained. Almeida *et al.* [1] provides more detailed results and interpretations, for the three embedment lengths, together with derived profiles for bond stress along the rebar lengths.

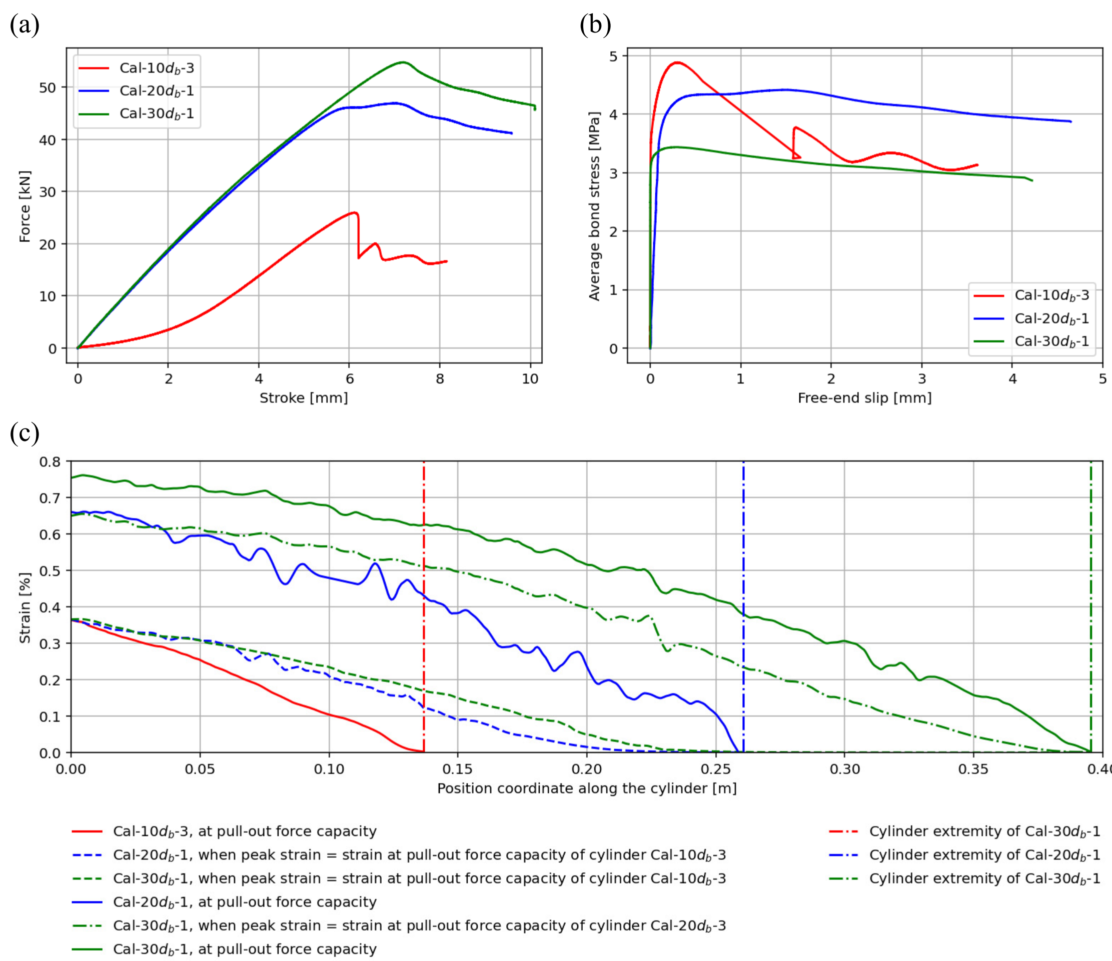

Figure 6. (a) Pull-out results for the cylindric samples 10d_b-20d_b-30d_b equipped with DFOS: (a) Force *versus* stroke; (b) Average bond stress *versus* free-end slip; (c) Strain profiles along the three rebars' lengths, at different strain demands (see legend), as measured by the DFOS.

5. Conclusions

The present experimental investigation addressed the effect of surface conditions, as well as the influence of embedment length ($L_e = 10d_b$, $20d_b$, and $30d_b$), on the bond-slip behaviour of GFRP rebars. With reference to the former, the significant influence of the surface treatment was confirmed (more details in Section 4). New commercially-available surface finishes, such as peel-ply and peel-ply/grid, provided the lower values of bond strength. Although not shown in this study, calendering surfaces showed even lower values. In comparison with an extended database from other studies, the current bond strength results are, overall, on the low side. Additionally, increasing the rebar diameter resulted in a larger bond strength, which is at odds with literature findings.

Another important aspect of novelty was introduced in the study of the influence of the embedment length on the bond-slip response (refer to Section 5): spatially-refined strain measurements along rebars were performed with distributed fibre optic sensors, for the first time in the literature for GFRP bond tests as far as the authors are aware. This provided novel insights into the bond-slip response, including the progressive nonlinearity of the strain profiles for longer embedment lengths at peak pull-out force. Even below this value, at identical values of pull-out forces, the bond stress seems to be more widely spread across the rebar for longer embedment lengths. For the reader interested in more details, a much-extended version of the tests and results shown herein can be found elsewhere [1].

Acknowledgments

The authors extend their gratitude to Arkema, particularly Pierre Gerard, for their support and providing the rebars, and to their colleagues at LEMSC – Catherine Doneux, Alex Bertholet, and Vincent Forzee – for their collaboration in the management and execution of the experimental tests.

References

[1] Almeida, J. P., Hoult, R., & Zoller, A. (2025). Effect of surface treatments and fiber-optic strain-sensed embedment length on the bond-slip behaviour of GFRP rebars, *Construction and Building Materials* (to be submitted).
[2] Zhao, X., Rahman, M. M., D'Antino, T., Focacci, F., & Carloni, C. (2022). Effect of bonded length on the load response and failure mode of pull-out tests of GFRP bars embedded in concrete, *Construction and Building Materials*, 347.
[3] Wambeke, B. W., & Shield, C. K. (2006). Development length of glass fiber-reinforced polymer bars in concrete, *ACI Structural Journal*, 103(1), 11–17.
[4] Solyom, S., & Balázs, G. L. (2020). Bond of FRP bars with different surface characteristics, *Construction and Building Materials*, 264.
[5] Aiello, M. A., Leone, M. and Pecce, M. (2007). Bond performances of FRP rebars-reinforced concrete, *Journal of Materials in Civil Engineering*, 19(3), 205–213.
[6] Wang, J., Xiao, F., Lai, Z., Yang, J., & Tian, S. (2024). Bond of FRP bars with different surface characteristics to concrete, *Structures*, 59.
[7] Ahmad, F. S., Foret, G., & Le Roy. R. (2011). Bond between carbon fibre-reinforced polymer (CFRP) bars and ultra high performance fibre reinforced concrete (UHPFRC): Experimental study, *Construction and Building Materials*, 25(2), 479–485.
[8] Benmokrane, B., Tighiouart. B., & Chaallal, O. (1996). Bond strength and load distribution of composite GFRP reinforcing bars in concrete, *ACI Materials Journal*, 93(3), 254–259.
[9] Zoller, A., Escalé, P. & Gérard, P. (2019). Pultrusion of bendable continuous fibers reinforced composites with reactive acrylic thermoplastic ELIUM® Resin, *Frontiers in Materials*, 6.
[10] ISO 10406-1 (2015). *Fibre-reinforced polymer (FRP) reinforcement of concrete - Test methods - Part 1: FRP bars and grids*.
[11] Hoult, R., Bertholet, A., & Almeida, J. P. (2023). Core versus surface sensors for reinforced concrete structures: A comparison of fiber-optic strain sensing to conventional instrumentation," *Sensors*, 23(3).
[12] Nepomuceno, E., Sena-Cruz, J., Correia, L., & D'Antino, T. (2021). Review on the bond behavior and durability of FRP bars to concrete, *Construction and Building Materials*, 287.